# Building a polarizable pair interaction potential for lanthanoids(III) in liquid water: A molecular dynamics study of structure and dynamics of the whole series

Magali Duvail, Pierre Vitorge,[a)] and Riccardo Spezia[b)]

*Laboratoire Analyse et Modélisation pour la Biologie et l'Environnement, CNRS UMR 8587, Université d'Evry Val d'Essonne, Boulevard F. Mitterrand, 91025 Evry Cedex, France*

In this work we have extended our previously presented polarizable pair interaction potential for $La^{3+}$-water [Duvail *et al.*, J. Chem. Phys. **127**, 034503 (2007)] to the whole lanthanoid(III) series ($Ln^{3+}$) interacting with water. This was performed taking into account known modification of ionic radius and atomic polarizability across the series and thus changing potential parameters according to that. Our procedure avoids the hard task of doing expensive high level *ab initio* calculations for all the atoms in the series and provides results in good agreement with experimental data and with *ab initio* calculations performed on the last atom in the series ($Lu^{3+}$, the atom for which the extrapolation should be in principle much crude). Thus we have studied the hydration properties of the whole $Ln^{3+}$ series by performing classical molecular dynamics in liquid phase. This systematic study allows us to rationalize from a microscopic point of view the different experimental results on $Ln^{3+}$-water distances, first shell coordination numbers and first shell water self-exchange reactivity. In particular, we found that across the series the coordination number decreases from 9 for light lanthanoids to 8 for heavy lanthanoids in a continuous shape. This is due to the continuous changing in relative stability of the two forms that can be both populated at finite temperature with different probabilities as a function of the $Ln^{3+}$ atomic number. The changeover of the $Ln^{3+}$ ionic radius across the series resulted to be the main driving physical properties governing not always the $Ln^{3+}$-water distance changing across the series but also the observed coordination number and consequently ligand dynamics. © *2009 American Institute of Physics.* [DOI: 10.1063/1.3081143]

## I. INTRODUCTION

Understanding the hydration behavior of heavy metal cations is a first step to understand their different physical and chemical properties in aqueous solution. To obtain a clear picture of ions hydration and more in general complexation, theoretical calculations and experiments are often done in a close connection.[1–5] In particular molecular dynamics (MD), using classical, *ab initio* or mixed quantum/classical interaction potential, is a method of choice since it is able to mimic real conditions that are crucial to determine structural and dynamical properties, i.e., bulk conditions and finite temperature.[6–12]

Among the interesting hydrated heavy metal cations, lanthanoids trications ($Ln^{3+}$) belong a chemical series which hydration properties are of particular interest, for both fundamental and applicative reasons: (i) questions about their coordination number (CN) behavior, and related three-dimensional structure, across the series are still at the center of recent research works,[13,14] (ii) they are chemical analogs of actinides(III) and understanding their hydration and complexation properties is important to design efficient proce-

dures able to separate lanthanoids(III) from actinides(III)—that are not only chemically but also radioactively toxic elements.[15–17]

$Ln^{3+}$-water distance decreases in an almost continuous way across the series and the first shell CN passes from nine for the light atoms to eight for the heavy ones.[13] To explain this passage was long ago proposed the so-called gadolinium break model by Spedding and co-workers.[18–20] In the 1990s Helm and co-workers[21,22] proposed a model for which the passage is not an abrupt changing but a progressive stabilization of the eightfold structure with respect the ninefold one, identifying the $Eu^{3+}$ as the turning point, such that for this cation in solution one should find a thermal equilibrium between the two forms leading to a CN of 8.5. Last experimental results of Persson *et al.*,[14] based on accurate surface-extended x-ray-absorption fine structure (EXAFS) analysis, proposed a similar model with no sudden change in hydration number across the series but a decreasing starting at $Ho^{3+}$.

MD is, in principle, one of the most adapted tool to clarify the $Ln^{3+}$ hydration behavior along the series. At this aim, a well suited $Ln^{3+}$-water interaction potential is needed. In past years, classical potentials were proposed by different authors studying mainly one single atom in the series at a time.[23,24] Other authors have studied three atoms in the series, taken at the beginning, in the middle, and at the end of

---
[a)]Also at CEA Saclay, DEN/DPC/SECR/LSRM, 91991 Gif Sur Yvette, France.
[b)]Author to whom correspondence should be addressed. Electronic mail: riccardo.spezia@univ-evry.fr. FAX: (+33) 1 69 47 76 55.
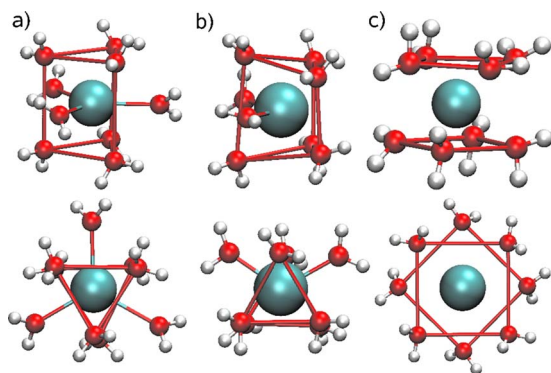
FIG. 1. (Color online) First hydration shell structures of hydrates lanthanoids(III): (a) TTP, for CN=9, (b) BTP, for CN=8, and (c) SAP for CN =8. Both top and side views are shown.

the series in order to catch fundamental specificities and building first pictures of $Ln^{3+}$ series hydration behavior. Their potentials are obtained from *ab initio* calculations, namely, they parametrized separately each cation such that reference *ab initio* $Ln^{3+}$-water potential energy curves were needed. Among these studies, the pioneering work of Kowall *et al.*,[25,26] done on $Nd^{3+}$, $Sm^{3+}$ and $Yb^{3+}$ found the change-over of the CN between 9 and 8 across the series. On the other hand, a most recent study of Floris and Tani[27] did not find such a behavior studying $Nd^{3+}$, $Gd^{3+}$, and $Yb^{3+}$—for which they found CN=8.9, 8.8, and 8.8, respectively. More recently, density-functional-theory-based *ab initio* calculations were performed on some $Ln^{3+}$ but since the limitations in simulation time length, they cannot fully study the hydration behavior across the series that is strictly connected to water exchange reaction occurring on a longer time scale.[28,29] A full systematic study of the hydration properties of the whole lanthanoid series by MD is thus still needed to obtain a full and coherent picture.

The study of water self-exchange mechanism in the series was performed by Cossy *et al.*[22,30] about 10 years ago, finding that rate constant increases across the series up to $Gd^{3+}$ and then it decreases. By inspecting the activation volume obtained for heavy lanthanoids, they proposed that the water self-exchange reaction proceeds via a concerted-associative mechanism for the CN=8→CN=9 reaction.[13] This mechanism holds for heavier lanthanoids where CN =8 is predominant, while for lighter $Ln^{3+}$ the water self-exchange was supposed to proceed through the corresponding concerted-dissociative mechanism. Of course, their interpretation of self-exchange mechanism and corresponding rate constants is based on assumptions on CN and microscopic structure of the first hydration shell, thus strengthening the importance of a having a clear microscopic picture of $Ln^{3+}$ hydration.

$[Ln(H_2O)_9]^{3+}$ structures present a tricapped trigonal prism (TTP) geometry [shown in Fig. 1(a)], as found in solid and liquid state by both experimental and theoretical studies,[13,21,22,31–34] while for $[Ln(H_2O)_8]^{3+}$ structures two geometries are possible: the bicapped trigonal prism (BTP) [see also Fig. 1(b)] that is the TTP structure where one equatorial water molecule left, and the square antiprism (SAP) geometry [also shown in Fig. 1(c)] where the four Ln–O distances

are equivalent. Classical MD done on $Yb^{3+}$ proposed that the CN=8 structure has a SAP geometry,[25] the same structure obtained for $Y^{3+}$ by experimental and theoretical studies.[28,35] On the other hand, recent EXAFS studies performed by Persson *et al.*[14] proposed that the heavy lanthanoids with CN =8 have a structure similar to CN=9 where equatorial water molecules are weaker bound to the lanthanoids, thus dealing to a structure more similar to the BTP.

We have recently proposed a pair interaction potential including explicit polarization to study $La^{3+}$ hydration[34] that was also in good agreement with EXAFS $K$-edge experiments.[36] In a recent communication we have proposed a set of modified parameters to use the same form to the whole series, finding a good agreement with experimental results and proposing a dynamical model to explain the hydration behavior along the series.[37] In particular, we have proposed that a changing in statistical predominance between the ninefold and eightfold structures governs the observed modified properties along the series, connecting structural and dynamical observations.

In the present work, we show and discuss in details the developing of our polarizable potential for all the series. This potential was essentially derived from the one proposed by us for $La^{3+}$ and extended to the whole series taking into account the known modifications of ionic radius and polarizability along the series. In order to do this extrapolation, some assumptions were done and verified *a posteriori* by comparing our results with *ab initio* calculations for the last atom in the series ($Lu^{3+}$) and finally with experiments in bulk water for the whole series. In particular, Ln–O distances were considered as the key quantities to compare with experiments since they are the most precise information that can be derived from EXAFS experiments—more than CNs. Our approach allows us to quickly derive potential parameters for the $Ln^{3+}$ series without doing *ab initio* calculations in order to do the parametrization, which has two advantages: (i) we avoid problematic and high computing resources demanding *ab initio* calculations on $Ln^{3+}$ that are open shell systems and probably need multireference calculations, (ii) since the potential is directly related to physical properties thus also simulation results can be explained in terms of those properties.

The outline of the reminder of the text is as follows. We first describe our potential development procedure (Sec. II), describing the method (Sec. II A), details on computations (Sec. II B) and properties obtained for $Lu^{3+}$ (Sec. III) that are compared to *ab initio* calculations in cluster phase and experiments in liquid phase. Then we show our systematic study of the hydration of the whole lanthanoids(III) series (Sec. IV), first discussing about the choice of physical parameters to use (Sec. IV A), then we describe structural (Sec. IV B) and dynamical (Sec. IV C) results. Section V summarizes and concludes.

## II. DEVELOPING WATER-LANTHANOIDS(III) INTERACTION POTENTIAL

### A. Methods

The total potential energy of our system is modeled as a sum of different terms,

$$V_{tot} = V_{elec} + V^{LJ}_{O-O} + V_{Ln-O}, \tag{1}$$

where $V_{elec}$ is the electrostatic energy term composed by a Coulomb and a polarization term following Thole's induced dipole model.[38] $V^{LJ}_{O-O}$ is the 12–6 Lennard-Jones potential describing the O–O interaction. Because of the explicit polarization introduced in the model, the original TIP3P water[39] was modified into the TIP3P/P water model,[34] i.e., the charges on O and H were rescaled to reproduce correctly the dipole moment of liquid water.

$V_{Ln-O}$ account for the *nonelectrostatic* Ln–O interaction potential. We have chosen a potential composed by a long range attractive part with a $1/r^6$ behavior and a short range repulsive part modeled via an exponential function, dealing with the well-known Buckingham exponential-6 potential (Buck6),

$$V^{Buck6}_{ij} = A_{ij} \exp(-B_{ij}r_{ij}) - \frac{C_{ij}}{r^6_{ij}}. \tag{2}$$

This potential, taking into account terms not explicitly included in the Coulomb and polarization part, was found to better reproduce $La^{3+}$-water properties.[34] The Ln–O Buck6 parameters are estimated from extrapolating the original La–O Buck6 parameters that were obtained by fitting the Møller–Plesset perturbation (MP2) potential energy curve.[34] Note that this expression was initially preferred to the common Lennard-Jones expression since a better fitting of the MP2 curve. This can be due to the higher flexibility of the exponential expression of the repulsive term but also to the more physical basis of the exponential form in treating short-range interactions.[40,41] The new potential energy is modified to be extensible to the whole series taking into account two physical properties that are known to change across the series: atomic polarizability and ionic radius.

Atomic polarizability directly enters in the polarization part of the electrostatic energy term and we use values reported in Ref. 42. The remaining part of the potential is the Buck6 potential where three parameters enter to determine the energy values: $A_{ij}$, $B_{ij}$, and $C_{ij}$. The first parameter, $A_{ij}$, represents the height of the Buckingham repulsion. This value is a fictitious value that for $La^{3+}$ is $1.004 \times 10^{+6}$ kJ mol$^{-1}$ corresponding to energies largely bigger than those explored in liquid phase. Thus, as often done in classical parametrizations, it is kept fixed through the series. The other two terms are modified following the changeover of ionic radius across the series. The $C_{ij}$ term was determined graphically as follows: assuming that the heights of the repulsion walls are the same for every $Ln^{3+}-OH_2$ interaction, then the new Ln curves are shifted toward smaller value considering difference in ionic radius with respect the $La^{3+}$ that is taken as the reference. In Fig. 2 we show the $Lu^{3+}-OH_2$ case. To modify the $B_{ij}$ term we have employed an empirical relationship that connects the term to the modification of ionic radius across the series

$$B_{LnO} = B_{LaO} + k\Delta r, \tag{3}$$

where $B_{LaO}$ is 3.48 Å$^{-1}$, as previously obtained, $\Delta r$ is the difference in ionic radius between $La^{3+}$ and the given $Ln^{3+}$ and $k$ is a proportionality factor that here is assumed to be
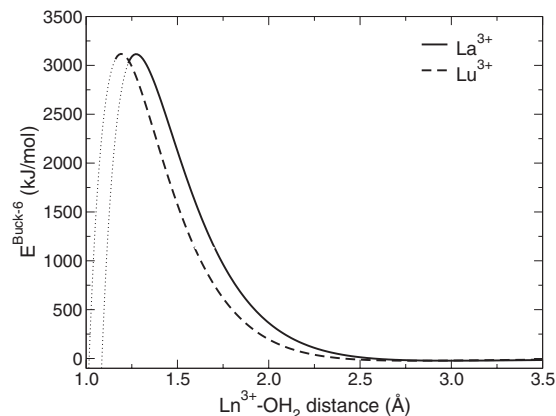


FIG. 2. Buck-6 energies curves for the $La^{3+}-OH_2$ (solid line) and the $Lu^{3+}-OH_2$ (dashed line) interactions.

1 Å$^{-2}$. This is a totally arbitrarily assumption that is verified *a posteriori* testing the new potential toward *ab initio* calculations—done for $Lu^{3+}$—and comparing MD data toward experiments. Lanthanoids polarizabilities were taken from Shannon[43] radii. Note that ionic radii, in solid phase, reported by Shannon are a function of the number of oxygen atoms around the lanthanoid. Here we have taken as reference the $La^{3+}$ ionic radius corresponding to a ninefold structure, i.e., 1.216 Å, and for the other lanthanoids we have taken the ninefold values for the lighter ones and both ninefold and eightfold values for heavier atoms, thus we have for each $Ln^{3+}$ heavier than $Pm^{3+}$ a double set of parameters, called hereafter $Ln^{3+}_{(9)}$ and $Ln^{3+}_{(8)}$, respectively. We will discuss details in Sec. IV A. Obtained $B_{ij}$ and $C_{ij}$ parameters, ionic radii, and polarizabilities used to obtain the potential for the whole series are listed in Table I. Note that this attempt to construct a potential which systematically depends on lanthanoid radius is very similar to what done by Madden and co-workers[44,45] in the case of molten salts.

## B. Computational details

Simulations of the hydrated $Ln^{3+}$ ions have been carried out in the microcanonical *NVE* ensemble with our own developed classical molecular dynamics (CLMD) code MDVRY,[46] using a Car–Parrinello-like scheme to obtain atomic induced dipoles.[47] The induced dipoles are obtained at the beginning of the dynamics through the resolution of the self-consistent equation

$$\mathbf{p_i} = \bar{\bar{\alpha}}_\mathbf{i} \cdot \left( \mathbf{E_i} + \sum_{\mathbf{i} \neq \mathbf{j}} \bar{\bar{\mathbf{T}}}_\mathbf{ij} \cdot \mathbf{p_j} \right), \tag{4}$$

where $\mathbf{p_i}$ is the induced dipole associated with an isotropic atomic polarizability tensor $\bar{\bar{\alpha}}_i$, following Thole's induced dipole model[38] and

$$\bar{\bar{T}}_{ij} = \frac{1}{r^3_{ij}} \left( \bar{\bar{1}} - 3\frac{\bar{\bar{A}}_{ij}}{r^2_{ij}} \right), \tag{5}$$

TABLE I. Parameters used for the CLMD simulations. $Ln^{3+}_{(9)}$ and $Ln^{3+}_{(8)}$ are model lanthanoids where we used ionic radii for extrapolation from experimental values corresponding to CN=9 and CN=8, respectively. Ionic radii are in angstrom, $B$ in $Å^{-1}$, $C$ in kJ $mol^{-1}$ $Å^6$ and atomic polarizabilities ($\alpha$) in $Å^3$.

| Ion | Ionic radius[a] | $B_{ij}$ | $C_{6,ij}/10^{+4}$ | $\alpha$[b] |
|---|---|---|---|---|
| $La^{3+}_{(9)}$ | 1.216 | 3.480 | 3.766 | 1.41 |
| $Ce^{3+}_{(9)}$ | 1.196 | 3.500 | 3.628 | 1.35 |
| $Pr^{3+}_{(9)}$ | 1.179 | 3.517 | 3.535 | 1.29 |
| $Nd^{3+}_{(9)}$ | 1.163 | 3.533 | 3.435 | 1.23 |
| $Pm^{3+}_{(9)}$ | 1.148[c] | 3.548 | 3.353 | 1.21[c] |
| $Pm^{3+}_{(8)}$ | 1.093[c] | 3.603 | 3.054 | 1.21[c] |
| $Sm^{3+}_{(9)}$ | 1.132 | 3.564 | 3.264 | 1.17 |
| $Sm^{3+}_{(8)}$ | 1.079 | 3.617 | 2.975 | 1.17 |
| $Eu^{3+}_{(9)}$ | 1.120 | 3.576 | 3.198 | 1.11 |
| $Eu^{3+}_{(8)}$ | 1.066 | 3.630 | 2.912 | 1.11 |
| $Gd^{3+}_{(9)}$ | 1.107 | 3.589 | 3.130 | 1.06 |
| $Gd^{3+}_{(8)}$ | 1.053 | 3.643 | 2.851 | 1.06 |
| $Tb^{3+}_{(9)}$ | 1.095 | 3.601 | 3.059 | 1.01 |
| $Tb^{3+}_{(8)}$ | 1.040 | 3.656 | 2.791 | 1.01 |
| $Dy^{3+}_{(9)}$ | 1.083 | 3.613 | 3.007 | 0.97 |
| $Dy^{3+}_{(8)}$ | 1.027 | 3.667 | 2.732 | 0.97 |
| $Ho^{3+}_{(8)}$ | 1.015 | 3.681 | 2.686 | 0.94 |
| $Er^{3+}_{(8)}$ | 1.004 | 3.692 | 2.640 | 0.90 |
| $Tm^{3+}_{(8)}$ | 0.994 | 3.702 | 2.598 | 0.86 |
| $Yb^{3+}_{(9)}$ | 1.042 | 3.654 | 2.810 | 0.80 |
| $Yb^{3+}_{(8)}$ | 0.985 | 3.711 | 2.565 | 0.80 |
| $Lu^{3+}_{(9)}$ | 1.032 | 3.667 | 2.751 | 0.77 |
| $Lu^{3+}_{(8)}$ | 0.997 | 3.719 | 2.527 | 0.77 |

[a]From Ref. 43.
[b]From Ref. 42.
[c]As the Pm element does not exist as a natural element, the ionic radius and the atomic polarizability are linearly extrapolated.

$$\bar{\bar{A}}_{ij}$$

$$= \begin{pmatrix} (x_i - x_j)^2 & (x_i - x_j)(y_i - y_j) & (x_i - x_j)(z_i - z_j) \\ (x_i - x_j)(y_i - y_j) & (y_i - y_j)^2 & (y_i - y_j)(z_i - z_j) \\ (x_i - x_j)(z_i - z_j) & (y_i - y_j)(z_i - z_j) & (z_i - z_j)^2 \end{pmatrix}.$$
(6)

The resolution of self-consistent problem becomes rapidly extremely time consuming as the system grows. Thus, to reduce computing time, we have used a Car–Parrinello type of dynamics of additional degrees of freedom associated with induced dipoles. The Hamiltonian of the system becomes

$$\mathcal{H} = V + \frac{1}{2}\sum_i m_i \mathbf{v}_i^2 + \frac{1}{2}\sum_{\mathbf{i}} \mathbf{m}_{\mathbf{p_i}} \mathbf{v}_{\mathbf{p_i}}^2,$$
(7)

where $V$ is the total potential, $\mathbf{v}_i$ is the velocity of the atom $i$, $\mathbf{v}_{\mathbf{p_i}}$ is the velocity of the induced dipole $\mathbf{p_i}$ treated as an additional degree of freedom in the dynamics, and $m_{\mathbf{p_i}}$ is its associated fictious mass (identical for each atom). Note that the dynamics of the induced dipole degrees of freedom is fictitious, such that it only serves the purpose of keeping the induced dipoles close to their values at the minimum energy (that would be obtained through the exact resolution of self-consistent equation at each step).

CLMD simulations were performed for one $Ln^{3+}$ and 216 rigid water molecules in a cubic box at room temperature. As previously reported,[34] test simulations with a 1000 water molecules box provide the same results and thus we used this relatively small box to simulate many systems with also different sets of parameters for each system. Simulations were done on a 2.4 GHz AMD Opteron CPU and each simulation takes about 10 h/ns.

Periodic boundary conditions were applied to the simulation box. Long-range interactions have been calculated by using smooth particle mesh Ewald method.[48] Simulations were performed using a velocity-Verlet-based multiple time scale for the simulations with the TIP3P/P water model. Equations of motion were numerically integrated using a 1 fs time step. The system was equilibrated at 298 K for 2 ps. Production runs were subsequently collected for 3 ns. The average temperature was 293 K with a standard deviation of 10 K. All simulations details are the same as reported previously.[34,37,49] Starting simulation boxes were build from a 216 equilibrated water box in which the ion was included at the center of the box. Regular tests on the equilibration doing 3 ns simulations also using as starting structure the one obtained after 1 ns simulations. The resulting radial distribution functions (RDFs) and angular distribution functions (ADFs) were calculated and they provided the same results, this giving us confidence in using an equilibration time of 2 ps for the full set of simulations.

*Ab initio* calculations were performed using the GAUSSIAN-98 package[50] at the MP2 level of theory. The La and Lu atoms were described by the Stuttgart/Dresden SDD basis set and the associated pseudopotentials. Hydrogen and oxygen atoms were described by the $6\text{-}31G^*$ basis set.[51]

## III. $Lu^{3+}$ HYDRATION PROPERTIES

### A. $Lu^{3+}$-water interaction energies in model clusters

The validity of the Lu–O Buck6 parameters determination was first checked by comparing *ab initio* and the model energies. The energy calculations were performed on the $La(H_2O)_9^{3+}$ and $Lu(H_2O)_8^{3+}$ clusters (Fig. 1), representing hydration shells of $La^{3+}(CN=9)$ in the TTP and $Lu^{3+}(CN=8)$ in the SAP geometries.

The extrapolation procedure was first tested for $Lu^{3+}$, the last atom in the series. $Lu^{3+}$ was chosen because it is the further atom in the series from $La^{3+}$ that is the reference atom and, being closed shell, *ab initio* calculations can be performed easily. Since for $Lu^{3+}$ the CN is well known to be eight, the parameters used here are those of $Lu^{3+}_{(8)}$. The validity of our model was further evaluated by comparing MP2 energies calculated as follows:

$$E^{MP2}_{Lu(H_2O)_8^{3+}} = E_{MP2} - E_{Lu^{3+}} - 8E_{H_2O},$$
(8)

$$E^{MP2}_{Lu^{3+}\text{-water}} = E_{MP2} - E_{Lu^{3+}} - E_{(H_2O)_8},$$
(9)

where $E_{(H_2O)_8}$ is the single-point MP2 energy including all water molecules at the same coordinate as in the computation of $E_{MP2}$, with model calculated energies of the $Lu(H_2O)_8^{3+}$ cluster. A good agreement between MP2 and model energies
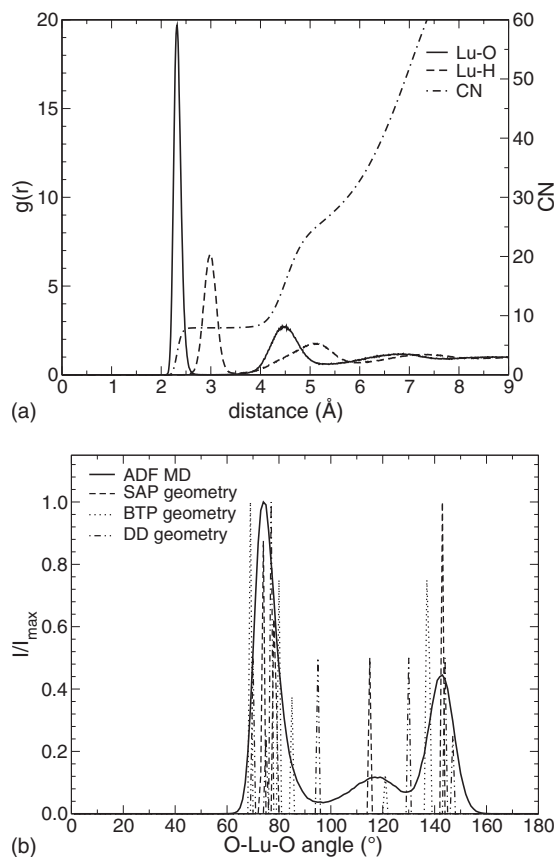
FIG. 3. Top: RDFs of Lu–O (solid line), Lu–H (dashed line), and CN (dashed-dotted line). Bottom: ADF of O–Lu–O in the first hydration shell (solid line) compared to ADF of the SAP (dashed line), BTP (dotted line), and DD (dotted-dashed line) geometries.

was obtained since we found $E^{MP2}_{Lu(H_2O)_8^{3+}}=-2305$ kJ mol$^{-1}$, $E^{MP2}_{Lu^{3+}\text{-water}}=-2496$ kJ mol$^{-1}$, and $E^{model}_{Lu(H_2O)_8^{3+}}=-2385$ kJ mol$^{-1}$. The same calculations were made for the La(H$_2$O)$_9^{3+}$ cluster and gave a difference of 128 kJ mol$^{-1}$ between $E^{MP2}_{La(H_2O)_9^{3+}}$ and model energies.[34] Thus, for the La(H$_2$O)$_9^{3+}$ cluster, the energy difference obtained by *ab initio* calculations and computed is of about 6%. Note that this result comes from the potential that was fitted on MP2 calculations, and being able to correctly reproduce MP2 energies for larger clusters and hydration in bulk water.[34,36] For the Lu(H$_2$O)$_8^{3+}$ cluster, this difference is of about 3% (80 kJ mol$^{-1}$), twice smaller than the one calculated for La$^{3+}$. This shows that the extrapolated potential gives results in good agreement with *ab initio* calculations, even better than those obtained for La$^{3+}$ that is our reference. This is a first indication that the extrapolation procedure can be a reasonable approximation that can be used to catch key solvation properties.

## B. Lu$^{3+}$ hydration structure in bulk water

Before studying the whole series, we present results of the extrapolated Lu$^{3+}_{(8)}$-water potential for bulk water hydration. In Fig. 3 Lu–O and Lu–H RDFs show two well-defined peaks corresponding to the two first hydration shells. The first and second peaks are centered at 2.32 and 4.50 Å, respectively (Table II), while the third hydration shell is not

well defined. As the other hydration shells are not defined, this means that Lu$^{3+}$ has an effect only on the first three hydration shells (to about 7.6 Å). Calculated Lu–O first hydration shell distance with the extrapolated Lu$^{3+}_{(8)}$-water potential is in good agreement with experimental values obtained by EXAFS spectroscopy [2.31,[52] 2.32,[53] 2.29,[14] 2.32,[14] and 2.34 Å (Ref. [54])] and x-ray diffraction (XRD) [2.34 (Ref. [55]) and 2.347 Å (Ref. [56])]. The first hydration shell CN is 8.01 that comes from a clear predominance of CN=8 structures, being in agreement with previously reported data.[13,55,57,58] In particular we found 98.9% of eight-fold configurations and 1.1% of ninefold ones.

Although no experimental data are available on the structural properties of the second hydration shell of Lu$^{3+}$, the Lu–O distance (4.50 Å) and CN (18.3), are consistent with the values obtained for the second hydration shell of La$^{3+}$.[34] Indeed, the difference between the calculated mean distance of the first hydration shell of La$^{3+}$ and Lu$^{3+}$ (0.2 Å) is of the same order of magnitude the one in the second hydration shell (about 0.15 Å). Note that the number of water molecules in the second hydration of Lu$^{3+}$ is similar to that calculated in the second hydration shell of La$^{3+}$, although the Lu–O second hydration shell distance is smaller than the La–O one. This means that Lu$^{3+}$ has more influence on the hydration properties than La$^{3+}$, originated by the fact that the Lu$^{3+}$ ion is smaller than the La$^{3+}$ ion with the same density of charge.

As mentioned above, the main CN calculated for the first hydration shell of Lu$^{3+}$ is 8. Contrary to a stoichiometry of 9, essentially described by the TTP geometry,[13,34] the stoichiometry of 8 can be described by several geometries: SAP, trigonal dodecahedron (DD), cubic, BTP.[59,60] However, although these geometries are close and quite difficult to determine, the SAP and DD are often used in literature to describe the first hydration shell of Lu$^{3+}$.[31,56] Different Lu–O distance values are often used to assign the structure since BTP has six distances with smaller values than the remaining two—a so-called 6+2 structure—the DD has four molecules at a shorter distance then the other four—a 4+4 structure—while in the SAP structure the four distances are equivalent. A typical way is to fit the Lu–O RDF of the first hydration shell with two Gaussian distribution functions. We have done it in three different ways: fixing the number of CNs to 6+2 and 4+4—corresponding to BTP and DD structure respectively—and fitting also the CN.

For the BTP geometry, we obtained two sets of distances at 2.30 Å for the six prismatic molecules ($r^P_{Lu-O}$) and 2.40 Å for the two capped molecules ($r^C_{Lu-O}$). Note that this geometry is very similar to the TTP geometry observed in the beginning of the lanthanoids series since the BTP geometry corresponds to the TTP geometry with a capped water molecule missing in the median of the prism. The ratio $r^C_{Lu-O}/r^P_{Lu-O}=1.043$ is of the same order of magnitude as the one calculated by Kowall *et al.*[26] (1.036) for the Nd(H$_2$O)$_9^{3+}$ complex, such that the structure can be seen as a BTP from this fitting.

On the other hand, for the DD geometry, we found four water molecules at a distance of 2.30 Å ($r^C_{Lu-O}$) and four at 2.36 Å ($r^P_{Lu-O}$). The ratio $r^C_{Lu-O}/r^P_{Lu-O}=1.026$ is in good

TABLE II. Hydration properties of $Ln^{3+}$ in aqueous solution at room temperature. $r_{Ln-O}$ is the maximum peak of the Ln-O RDFs (in angstrom), CN is the coordination number, and MRT is the mean residence time (in ps). [1] is for the first hydration shell and [2] for the second.

| Ion | $r_{Ln-O}^{(1)}$ | $CN^{(1)}$ | $MRT^{(1)}$ | $r_{Ln-O}^{(2)}$ | $CN^{(2)}$ | $MRT^{(2)}$ |
|---|---|---|---|---|---|---|
| $La_{(9)}^{3+}$ | 2.52 | 9.02 | 1082 | 4.65 | 18.8 | 7.6 |
| $Ce_{(9)}^{3+}$ | 2.50 | 9.00 | 1769 | 4.65 | 19.3 | 6.6 |
| $Pr_{(9)}^{3+}$ | 2.49 | 9.00 | 1912 | 4.64 | 19.3 | 6.2 |
| $Nd_{(9)}^{3+}$ | 2.48 | 9.00 | 1482 | 4.63 | 19.2 | 6.4 |
| $Pm_{(9)}^{3+}$ | 2.46 | 9.00 | 900 | 4.64 | 18.5 | 7.3 |
| $Pm_{(8)}^{3+}$ | 2.44 | 8.97 | 642 | 4.60 | 19.2 | 7.5 |
| $Sm_{(9)}^{3+}$ | 2.46 | 9.00 | 562 | 4.62 | 19.2 | 7.7 |
| $Sm_{(8)}^{3+}$ | 2.42 | 8.94 | 425 | 4.60 | 19.1 | 7.0 |
| $Eu_{(9)}^{3+}$ | 2.45 | 9.00 | 782 | 4.61 | 17.6 | 8.0 |
| $Eu_{(8)}^{3+}$ | 2.41 | 8.90 | 245 | 4.58 | 19.0 | 7.6 |
| $Gd_{(9)}^{3+}$ | 2.44 | 8.95 | 426 | 4.61 | 19.2 | 8.4 |
| $Gd_{(8)}^{3+}$ | 2.39 | 8.72 | 254 | 4.55 | 18.9 | 7.8 |
| $Tb_{(9)}^{3+}$ | 2.43 | 8.97 | 264 | 4.60 | 16.3 | 7.7 |
| $Tb_{(8)}^{3+}$ | 2.37 | 8.59 | 171 | 4.55 | 18.9 | 7.2 |
| $Dy_{(9)}^{3+}$ | 2.42 | 8.91 | 287 | 4.59 | 16.6 | 7.6 |
| $Dy_{(8)}^{3+}$ | 2.36 | 8.36 | 226 | 4.52 | 18.7 | 8.0 |
| $Ho_{(8)}^{3+}$ | 2.34 | 8.24 | 246 | 4.52 | 18.6 | 8.0 |
| $Er_{(8)}^{3+}$ | 2.33 | 8.14 | 351 | 4.51 | 18.7 | 8.8 |
| $Tm_{(8)}^{3+}$ | 2.33 | 8.06 | 527 | 4.50 | 18.3 | 8.9 |
| $Yb_{(9)}^{3+}$ | 2.36 | 8.33 | 228 | 4.53 | 19.4 | 10 |
| $Yb_{(8)}^{3+}$ | 2.32 | 8.02 | 665 | 4.49 | 18.3 | 9.2 |
| $Lu_{(9)}^{3+}$ | 2.35 | 8.24 | 152 | 4.52 | 18.4 | 9.7 |
| $Lu_{(8)}^{3+}$ | 2.32 | 8.01 | 1327 | 4.50 | 18.3 | 9.7 |

agreement with the one calculated by Rogers and Kurihara[56] (1.025) on the $Lu(H_2O)_8Cl_3 \cdot$ 15-crown-5 by XRD with a DD geometry, such that also the DD structure seems to be a possible structure from this Gaussian decomposition procedure.

Finally, we fitted the Lu–O RDF with two Gaussian distributions, obtaining CN=3.46 at $r_{Lu-O}^P$ 2.30 Å and CN =4.55 at $r_{Lu-O}^C$ 2.37 Å. The ratio of 1.030 that does not correspond to any structure—since the CNs do not—is between the theoretical values for BTP and DD, this probably meaning that this is not, in this case, the correct parameter to distinguish the structure. In particular, one should keep in mind that we are not dealing with crystals but with structures that thermally move in a liquid phase at finite temperature. The ADF, shown in Fig. 3, can help in determining the structure from a dynamical point of view. In the same figure we report the values corresponding to the perfect (and static) SAP, BTP, and DD structures. Note that the ADF peaks are at the same positions of the theoretical SAP values, with distributions due to thermal effects. On the other hand, ADF curve and BTP and DD theoretical values do not match. Thus, we can say that we have a SAP structure, where we have to keep in mind the dynamical meaning of a structure: for each snapshot a precise symmetry cannot be identified and only averages can correctly describe the structure. Thus, imposing a structure, then fitting the distances and comparing results with ideal crystals seems to be a misleading procedure in a dynamical context. The direct use of distributions, for distances and angles, seems to be the most correct approach in dynamical systems, where also results should be seen in a

dynamical way. Thus, a SAP structure, in this context, does not mean a perfect SAP structure but a SAP-like dynamical structure.

## C. Validation of the extrapolation procedure for $Lu^{3+}$

CLMD simulations of hydrated $Lu^{3+}$ were also performed using other atomic polarizability and other Buck6 parameters in order to understand the effect of parameters on resulting properties. We indeed performed CLMD simulations using the $La^{3+}$ atomic polarizability (1.41 Å$^3$) instead of the 0.77 Å$^3$ value and the initial Lu–O Buck6 parameters. Using this set of parameters, we found an increased Lu–O distance in the first coordination shell of 0.01 Å (2.33 Å instead of 2.32 Å). As a consequence of the increasing Lu–O distance in the first hydration shell, the CN passes from 8.01 to 8.13. Note that, from a structural point of view, we calculated the same structural properties of hydrated $Er^{3+}$ ($d_{Er-O}^{(1)}$ =2.33 Å and $CN^{(1)}$=8.14). This means that the CN depends directly to the first hydration shell distance.

As mentioned above, the determination of the $B_{Ln-O}^{Buck6}$ parameter was done taking into account the lanthanoid ionic radius variation across the series. For $Lu^{3+}$, it is well know that the CN in the first hydration shell is 8.[13,55,57,58] Thus, in a first parametrization, we have taken the ionic radius corresponding to a CN of 8 [$r_8^+$=0.977 Å (Ref. 43)] to obtain our parameters. When using those parameters on a simulation, even changing the polarizability, the resulting CN is always 8 or close to 8. To see the impact of ionic radius on results, we have considered also the ionic radius of $Lu^{3+}$ reported for a solid structure with CN=9 [$r_9^+$=1.032 Å (Ref. 43)]. Then
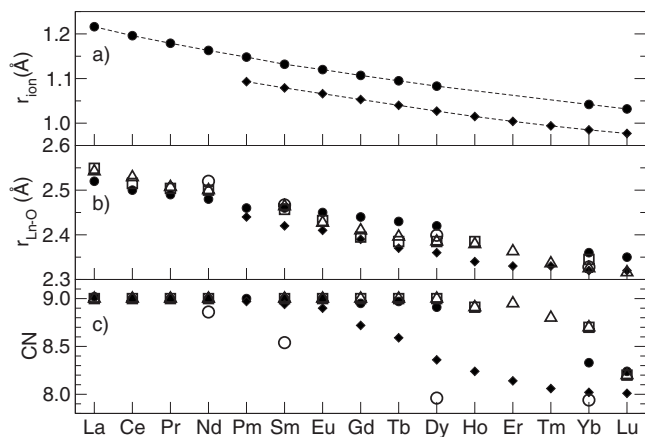
FIG. 4. (a) Ionic radius variation in the lanthanoid series used to extend the interaction potential corresponding to a CN of 9 (filled circles) and 8 (filled diamonds). (b) Variation of the first hydration shell distance as a function of the atomic number through the lanthanoid series. Results obtained with $Ln_{(9)}^{3+}$ parameters in filled circles and those with $Ln_{(8)}^{3+}$ parameters in filled diamonds. Experimental data are also shown: circles are neutron diffraction data from Ref. 22, squares are EXAFS $K$-edge data from Ref. 14, and triangles are EXAFS $L_{III}$-edge data from Ref. 14. (c) Variation of the first hydration shell CN as a function of the atomic number through the lanthanoids series. Symbols are the same of (b) panel.

CLMD simulations were performed using parameters reported in Table I. From this set of simulations we obtained a Lu–O distance in the first hydration shell of 2.35 with a CN of 8.24. In Table II we summarize all the results obtained with the CN=8 and CN=9 ionic radii, respectively, $Lu_{(8)}^{3+}$ and $Lu_{(9)}^{3+}$. Note that also using the $Lu_{(9)}^{3+}$ parameters the CN is 8 and values are closer to those in the series with a bigger ionic radius.

## IV. SOLVATION OF THE WHOLE LANTHANOID(III) SERIES

### A. Calibration of the interaction potential

Once the new potential tested for $Lu^{3+}$ hydration, we extended the extrapolation procedure to the whole lanthanoid series. The Buck6 parameters were thus estimated from the reported polarizabilities and ionic radii in the series. In the seminal Shannon work ionic radii are reported as a function of the CN (CN=8 or 9 for the $Ln^{3+}$ ion).[43] We can thus obtain two sets of parameters for the two CNs, $Ln_{(8)}^{3+}$ and $Ln_{(9)}^{3+}$. Values obtained are reported in Table I.

It is well established now that the CN is 9 and 8 for the beginning and the end of the series, respectively.[13,37,55,57,61] Thus, we used the ionic radii corresponding to CN=9 for the beginning, and 8 for the end of the series to calculate the Buck6 parameters. For the lanthanoids in the middle of the series, two stoichiometries [$Ln(H_2O)_8^{3+}$ and $Ln(H_2O)_9^{3+}$] coexist.[32,37] Thus, we have chosen ionic radii corresponding to CN=9 from $Ce^{3+}$ to $Dy^{3+}$. As discussed in the previous paragraph, also for $Lu^{3+}$ we have tested the $Ln_{(9)}^{3+}$ parameters and we have done the same also for the lanthanoid before $Lu^{3+}$, i.e., $Yb_{(9)}^{3+}$. From $Pm^{3+}$ to $Lu^{3+}$ we have calculated values corresponding to CN=8. Note that we have an overlapping region that corresponds to a region where the CN is not well defined. In Fig. 4(a) we show the used ionic radii and

atomic polarizabilities for each atom, where we specified the CN number used for the ionic radius.

Finally, we should choose one parameter for each lanthanoid and we will take the parameter that, used in CLMD simulations, will provide the better agreement with experimental results in terms of Ln–O distance. This choice is justified by the fact that the distance is the experimental data with smaller uncertainty. In Figs. 4(b) and 4(c) we report distances and CNs obtained for the different sets of parameters and compared with experimental data. All the details on first and second shell distances, CNs and mean residence times (MRTs) are reported in Table II. Considering Ln–O distances as the criterion parameter, we should say that the better agreement is obtained from $Ce_{(9)}^{3+}$ to $Sm_{(9)}^{3+}$ and from $Eu_{(8)}^{3+}$ to $Lu_{(8)}^{3+}$. The corresponding Buck6 parameters were used in Sec. IV B to discuss into details structural and dynamical lanthanoids properties. Before moving to this analysis we should pause and make some consideration on the ionic radius choice and on physical implication of these results.

First, we should note that choosing the ionic radius corresponding to CN=8 to obtain the Buck6 parameters, we did not find, necessarily, CN=8 from simulations. Indeed, $Eu_{(8)}^{3+}$ parameters provide a CN close to 9 (8.90), whereas the $Eu_{(9)}^{3+}$ ones a CN of 9.00 (Table II). The same observation can be done for the end of the series, where for $Yb^{3+}$ we obtained a CN of 8.02 and 8.33 using $Yb_{(8)}^{3+}$ and $Yb_{(9)}^{3+}$ parameters respectively.

Then we better investigated the role of ionic radius. Comparing the Ln–O distances in the first hydration shell as a function of the ionic radius, corresponding to CN=8 and CN=9, we observed that the distance varies almost linearly, as shown in Fig. 5. As expected, the structural hydration properties depend directly on the ionic radius, since for $Pm_{(8)}^{3+}$ and $Tb_{(9)}^{3+}$ ($r^+$=1.093 and 1.095 Å, respectively), we found the same Ln–O distances, i.e., 2.44 Å for $Pm_{(8)}^{3+}$, and 2.43 Å for $Tb_{(9)}^{3+}$, and consequently the same CN is found, as it depends on the Ln–O distance. This CN dependence on ionic radius is also clearly shown in Fig. 5 where CN is plotted as a function of ionic radius used for the parameters extrapolation.

These results strengthen the view that ionic radius is a key physical quantity playing a crucial role in determining lanthanoids hydration.

### B. Structural properties

As already mentioned, here and hereafter we discuss results obtained with the "better" set of parameters, i.e., $Ce_{(9)}^{3+}$–$Sm_{(9)}^{3+}$ and $Eu_{(8)}^{3+}$–$Lu_{(8)}^{3+}$. Thus, we remove (8) or (9) indices to simplify the notation.

Considering the $Ln^{3+}$ first hydration shell, we observed a linear decreasing of the Ln–O distances in the series [Fig. 4(b)], going from 2.52 Å for $La^{3+}$ to 2.32 Å for $Lu^{3+}$ (Table II). Note that the difference between the La–O and the Lu–O distance in the first hydration shell (0.20 Å) is almost equal to the difference between $La^{3+}$ and $Lu^{3+}$ ionic radii (0.22 Å), showing that the Ln–O distance is directly linked to the cat-
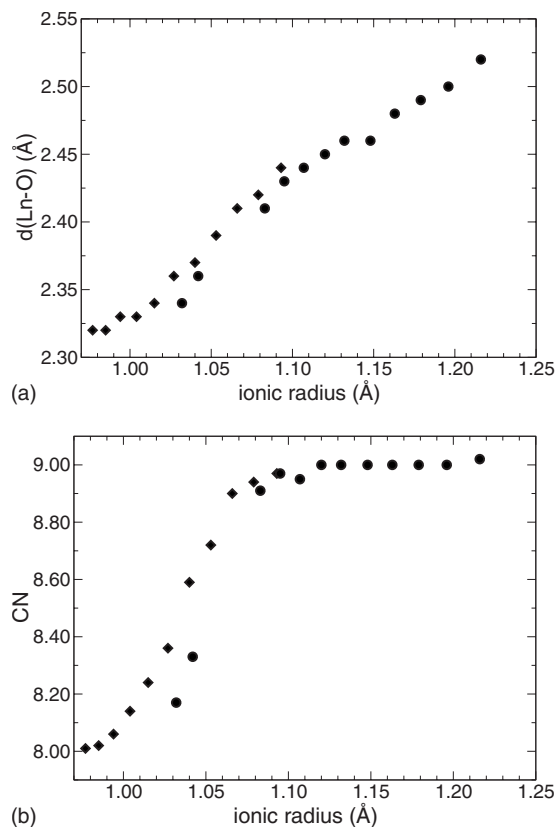
FIG. 5. Ln–O distances (upper panel) and CN (lower panel) as a function of ionic radii used for determining $B_{ij}$ and $C_{ij}$ of the model potential. Results obtained with $Ln_{(9)}^{3+}$ parameters in filled circles and those with $Ln_{(8)}^{3+}$ parameters in filled diamonds.

ion size. The calculated Ln–O distances in the first hydration shell are in good agreement with experimental values. Indeed, as an example, we can mention Ln–O distances of 2.48, 2.41, and 2.34 Å for $Nd^{3+}$, $Eu^{3+}$, and $Ho^{3+}$, respectively, being in good agreement with different EXAFS data,[52,62,63] Note that, the Buck6 parameters for the lanthanoid series, determined from the $La^{3+}$ Buck6 parameters, which gave a La–O distance slightly smaller than experimental value [2.52 Å instead of about 2.56 Å (Refs. [14], [33], and [63])], allow to determine Ln–O distances in better agreement with experiments for the end of the series.

As done in the EXAFS work of Persson *et al.*,[14] we fitted the first RDF Ln–O peak by one and two Gaussian functions, providing us one or two Ln–O distances in the first hydration shell, respectively. Considering the stoichiometries with 9 and 8 water molecules in the TTP and BTP geometries, respectively, the two fitted distances might correspond to the prismatic ($r_{Ln-O}^P$) and capped ($r_{Ln-O}^C$) Ln–O distances (Table III). As already remarked in Sec. III B, this can be a crude model and for heavier lanthanoids, as for $Lu^{3+}$, this distinction can be totally misleading. In any case we retain here the formal notation of prismatic for the water molecules closer to the cation and capped for the others. Results are shown in Table III and compared with corresponding experimental values reported by Persson *et al.*[14] both doing a one-shell and a two-shell fit.

Good agreements between the two Ln–O distances calculated from MD simulations and determined by EXAFS

spectroscopy are obtained. Calculated prismatic Ln–O distances are actually close to those determined experimentally, whereas we noticed that calculated capped distances are slightly smaller than those obtained by EXAFS, explaining the difference between the mean Ln–O distances calculated from MD simulations and determined by EXAFS. Furthermore, integrating the two Gaussian functions that fit the first hydration shell peak, allows us to determine two CNs corresponding to a prismatic ($CN^P$) and a capped ($CN^C$) CN. The calculated prismatic and capped CNs did not really give information on the geometry of the first hydration shell, since the $CN^P$ is not equal to 6—ideal value for TTP or BTP geometry—as previously noticed for $Lu^{3+}$. The mean $CN^P$ is actually of about 5 in the series. These values, not corresponding to any ideal symmetric structure, seem to reflect the fast interconversion between prismatic and capped position in a finite temperature dynamics. As already noticed, we are describing dynamical systems and averages should be considered to define a geometry.

Although the mean Ln–O distance in the first hydration shell varies linearly, the CN in this shell does not. Indeed, a sigmoid variation of the CN is observed, with an inflection point between $Tb^{3+}$ and $Dy^{3+}$ [Fig. 4(c)]. As found by Persson *et al.*,[14] the CN in the first hydration shell does not suddenly change from 9 to 8, as in the so-called gadolinium break model. However, although we observed the same shape of the CN as in their study, our model yielded a CN decreasing before in the series. Note that using $Ln_{(9)}^{3+}$ parameters we found that the CN sigmoid has the flex shifted toward heavier lanthanoids, thus more in agreement with these last experiments, as shown in Fig. 4(c). However, Ln–O distances are better reproduced by the other set of parameters, the $Ln_8^{3+}$ ones, for heavier lanthanoids and since Ln–O distances are more reliable in EXAFS experiments, we retain these last values for defining the "better" potential. We should pause to note that distances obtained for the "8" and "9" parameter sets are systematically too low or too high, respectively. The ion-oxygen distances shown in Fig. 4(b) obtained from different parameter sets suggest that an intermediate value could be chosen in the parametrization. This is beyond the aim of the present work—where we want to show the possibility of building a reliable potential starting from physical properties without an *a priori* knowledge of the results —but it can be the subject of a future work. In fact simulation results—structural as well as dynamical data, as we will see Sec. IV C—are strongly correlated with the chosen parametrization and using a parametrization based on a sort of intermediate values can be of significant importance.

The decreasing of the CN in the lanthanoid series and the corresponding modification in the first hydration shell structure is also observed from the O–Ln–O ADF, as shown in Fig. 6. At the beginning of the series, two peaks are observed centered at about 70° and 135°, corresponding to a TTP structure. Going to the end of the series, we observed that the two previous peaks are shifted through bigger angles (74° and 143° for $Lu^{3+}$), and a third peak appears at 118° from $Dy^{3+}$. The three peaks, mainly observed for heavy lanthanoids, are characteristic of the stoichiometry $Ln(H_2O)_8^{3+}$ in the SAP geometry, as shown on Fig. 3. Thus, the ADFs

TABLE III. Structural properties of the first hydration shell of $Ln^{3+}$ at room temperature determined by means of two models: one-shell model with an average of $Ln^{3+}$ distance, and two-shell model taking into account capping and prismatic water molecules. $EXAFS^K$ are $K$-edge absorption results from Ref. 14 and $EXAFS^L$ are $L_{III}$-edge absorption results from Ref. 14.

| Ion | Method | One shell fit | | | Two-shell fit | | |
|-----|--------|---------------|----|---------------|--------|---------------|--------|
| | | $r_{Ln-O}$ | CN | $r^P_{Ln-O}$ | $CN^P$ | $r^C_{Ln-O}$ | $CN^C$ |
| $La^{3+}$ | MD | 2.52 | 9.02 | 2.50 | 5.31 | 2.58 | 3.69 |
| | $EXAFS^K$ | 2.55 | 9 | 2.52 | 6 | 2.62 | 3 |
| | $EXAFS^L$ | 2.54 | 9 | 2.51 | 6 | 2.60 | 3 |
| $Ce^{3+}$ | MD | 2.50 | 9.00 | 2.48 | 5.1 | 2.56 | 3.9 |
| | $EXAFS^K$ | 2.51 | 9 | 2.51 | 6 | 2.59 | 3 |
| | $EXAFS^L$ | 2.53 | 9 | 2.49 | 6 | 2.60 | 3 |
| $Pr^{3+}$ | MD | 2.49 | 9.00 | 2.46 | 5.25 | 2.55 | 3.75 |
| | $EXAFS^K$ | 2.50 | 9 | 2.47 | 6 | 2.61 | 3 |
| | $EXAFS^L$ | 2.51 | 9 | 2.47 | 6 | 2.54 | 3 |
| $Nd^{3+}$ | MD | 2.48 | 9.00 | 2.46 | 5.1 | 2.54 | 3.9 |
| | $EXAFS^K$ | 2.50 | 9 | 2.45 | 6 | 2.56 | 3 |
| | $EXAFS^L$ | 2.50 | 9 | 2.46 | 6 | 2.57 | 3 |
| $Sm^{3+}$ | MD | 2.46 | 9.00 | 2.44 | 5.36 | 2.53 | 3.64 |
| | $EXAFS^K$ | 2.46 | 9 | 2.42 | 6 | 2.53 | 3 |
| | $EXAFS^L$ | 2.46 | 9 | 2.42 | 6 | 2.52 | 3 |
| $Eu^{3+}$ | MD | 2.41 | 8.90 | 2.40 | 5.48 | 2.49 | 3.42 |
| | $EXAFS^K$ | 2.43 | 9 | 2.41 | 6 | 2.52 | 3 |
| | $EXAFS^L$ | 2.43 | 9 | 2.41 | 6 | 2.52 | 3 |
| $Gd^{3+}$ | MD | 2.39 | 8.72 | 2.38 | 5.38 | 2.47 | 3.34 |
| | $EXAFS^K$ | 2.39 | 9 | 2.40 | 6 | 2.52 | 3 |
| | $EXAFS^L$ | 2.41 | 9 | 2.39 | 6 | 2.52 | 3 |
| $Tb^{3+}$ | MD | 2.37 | 8.59 | 2.36 | 5.46 | 2.44 | 3.13 |
| | $EXAFS^K$ | 2.38 | 9 | 2.38 | 6 | 2.49 | 3 |
| | $EXAFS^L$ | 2.40 | 9 | 2.39 | 6 | 2.51 | 3 |
| $Dy^{3+}$ | MD | 2.36 | 8.36 | 2.35 | 5.42 | 2.43 | 2.94 |
| | $EXAFS^K$ | 2.38 | 9 | 2.37 | 6 | 2.50 | 3 |
| | $EXAFS^L$ | 2.38 | 9 | 2.37 | 6 | 2.49 | 3 |
| $Ho^{3+}$ | MD | 2.34 | 8.24 | 2.33 | 4.97 | 2.41 | 3.27 |
| | $EXAFS^K$ | 2.38 | 8.91 | 2.37 | 6 | 2.49 | 2.91 |
| | $EXAFS^L$ | 2.38 | 8.91 | 2.37 | 6 | 2.50 | 2.91 |
| $Er^{3+}$ | MD | 2.33 | 8.14 | 2.33 | 5.19 | 2.40 | 2.95 |
| | $EXAFS^L$ | 2.36 | 8.95 | 2.35 | 6 | 2.46 | 2.95 |
| $Tm^{3+}$ | MD | 2.33 | 8.06 | 2.31 | 4.69 | 2.38 | 3.37 |
| | $EXAFS^L$ | 2.34 | 8.80 | 2.33 | 6 | 2.45 | 2.80 |
| $Yb^{3+}$ | MD | 2.32 | 8.02 | 2.30 | 4.59 | 2.37 | 3.43 |
| | $EXAFS^K$ | 2.34 | 8.70 | 2.32 | 6 | 2.43 | 2.70 |
| | $EXAFS^L$ | 2.32 | 8.70 | 2.31 | 6 | 2.42 | 2.70 |
| $Lu^{3+}$ | MD | 2.32 | 8.01 | 2.30 | 3.46 | 2.37 | 4.55 |
| | $EXAFS^K$ | 2.29 | 8.20 | 2.27 | 6 | 2.34 | 2.20 |
| | $EXAFS^L$ | 2.32 | 8.20 | 2.27 | 6 | 2.34 | 2.20 |
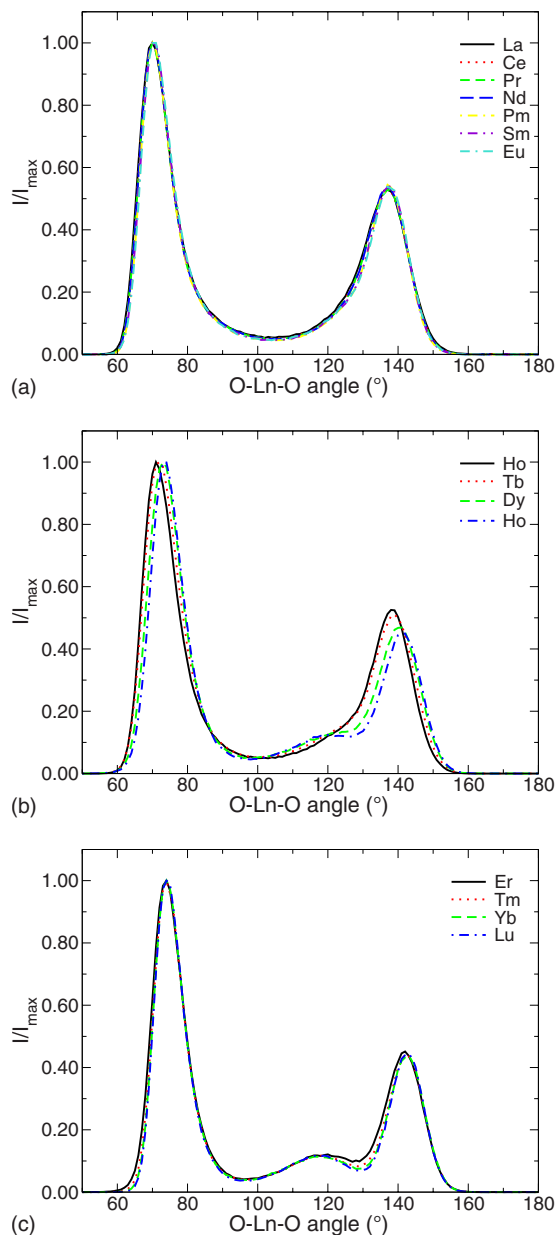
FIG. 6. (Color online) Evolution of the ADFs across the series: (a) from $La^{3+}$ to $Eu^{3+}$, (b) from $Gd^{3+}$ to $Ho^{3+}$, and (c) from $Er^{3+}$ to $Lu^{3+}$.



FIG. 7. Time evolution of the first hydration shell CN (CN) for $Nd^{3+}$, $Gd^{3+}$, $Ho^{3+}$, and $Lu^{3+}$.

allow us to conclude that the geometry at the beginning and at the end of series are TTP and SAP, respectively. In the middle of the series ADFs correspond to a mix between the TTP and SAP geometries, reflecting the dynamical coexistence between these two stoichiometries that we have already pointed out.[37]

## C. Dynamical properties

As mentioned above, water molecules exchanges between the first and the second hydration shells have been observed. Here, we present these water exchanges for some selected lanthanoids: $Nd^{3+}$ being a light lanthanoid, $Gd^{3+}$ and $Ho^{3+}$ located in the middle of the series, and $Lu^{3+}$ being the heaviest lanthanoid of the series. Water exchanges occurring in the first hydration shell of $Nd^{3+}$, mainly coordinated to 9 water molecules, lead to the formation of transient com-
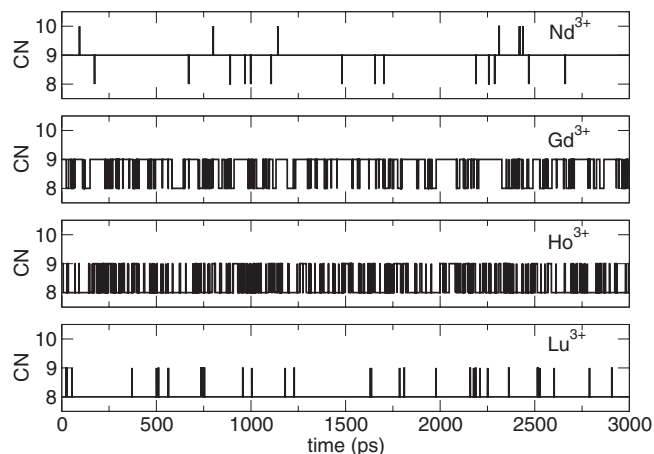
plexes $Nd(H_2O)_{10}^{3+}$ and $Nd(H_2O)_8^{3+}$ (Fig. 7), having small lifetimes (less than 10 ps), as already observed for $La^{3+}$.[34] For $Lu^{3+}$, mainly coordinated to 8 water molecules, the transient complex is $Lu(H_2O)_9^{3+}$, whereas for $Gd^{3+}$ and $Ho^{3+}$, no transient complexes are observed, since many fast exchanges occur during the simulation (Fig. 7).

As mentioned in our previous work, in the middle of the series the exchange frequency of water in the first hydration shell increases.[37] We do not observed a long lifetime of the $Ln(H_2O)_8^{3+}$ and $Ln(H_2O)_9^{3+}$ stoichiometries in the middle of the series since the MRTs of water molecules in that part of the series is five to ten times smaller than at the beginning or the end of the series, where main CNs are 9 and 8. The "direct" method[12] was used to determine the MRTs of water molecules. The MRTs were thus estimated from an average of the time spent by a water molecule in the first hydration shell. As usual, a minimum time parameter ($t^*=0.1$ ps) defining a real "exchange" was introduced. For consistency, the same protocol was used to estimate the MRTs for the second hydration shell.

The self-exchange mechanism can be in general associative ($A$), dissociative ($D$), and concerted ($I$), where the associative and dissociative ones can be concerted associative ($I_a$) and concerted dissociative ($I_d$). Of course to define a mechanism we should first define the CNs involved.

In Fig. 8 we show the time evolution of Nd–O distances with two water self-exchanges. We note that when a water molecule leaves another enters. Note that the formal CN $=10$ stoichiometry found corresponds to a very short time period where the leaving and the incoming water molecules are close to Nd. Exchange can happen also passing through a "formal" CN=8 structure, but in both cases we have that the leaving and the incoming water molecules are, for a very short time, in the first hydration shell. The mechanism seems thus to be concerted. Considering the reaction as a 9-8-9 reaction—as happens when CN=8 structures are found—the mechanism could be defined as concerted dissociative, while when the self-exchange reaction is 9-10-9, as for $La^{3+}$, the mechanism is concerted.

Regarding the Gd–O distance evolution as a function of the simulation time, it is difficult to define a self-exchange
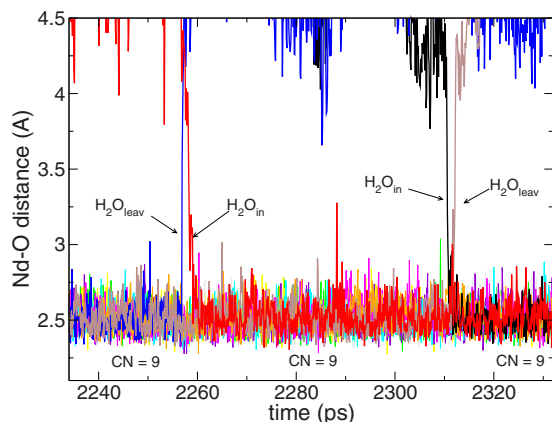
FIG. 8. (Color online) Nd–O distance of selected water molecules as a function of time.



FIG. 10. (Color online) Ho–O distance of selected water molecules as a function of time.

mechanism since the stoichiometries with 8 and 9 water molecules have almost the same lifetimes (Fig. 9). In this case, it is however difficult to decide unambiguously where the border lies between an exchange reaction and a dynamic equilibrium.

Although $Ho^{3+}$ is in the middle of the series, the water self-exchanges is a 8-9-8 reaction since the $Ho(H_2O)_9^{3+}$ complex has a short lifetime (2–5 ps) (Fig. 10). The mechanism seems to be concerted associative.

For $Lu^{3+}$ first hydration shell self-exchange, the reaction is also a 8-9-8, as shown in Fig. 11. Also in this case the mechanism seems to be concerted associative.

If we consider only 9-8-9 and 8-9-8 reactions, for light and heavy lanthanoids, respectively, it seems that concerted dissociative and associative exchanges can be highlighted for the beginning and the end of the lanthanoid series. On the other hand, for lanthanoids in the middle of the series, with $Ln(H_2O)_9^{3+}$ and $Ln(H_2O)_8^{3+}$ stoichiometries having almost the same lifetimes, no reaction pathway can be clearly proposed.

In all cases, water exchanges occurred always in the medium triangle, i.e., the ninth water molecule leaves and enters the first hydration by a capped position, as shown for $La^{3+}$.[34] As previously mentioned, going from the $Ln(H_2O)_9^{3+}$ to the $Ln(H_2O)_8^{3+}$ stoichiometry involves a change of geometry from TTP to SAP or BTP. Furthermore, from the values of the calculated capped and prismatic CNs, it seems that, for
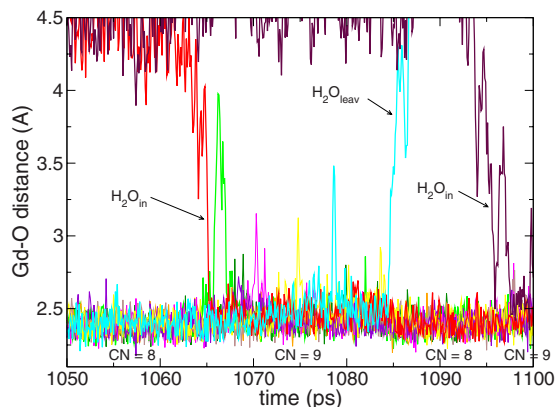
$Ln^{3+}$ at the very end of the series ($Tm^{3+}$–$Lu^{3+}$), the BTP geometry relaxes to the SAP geometry, since the $CN^P$ and $CN^C$ become closer (Table III). Thus, the geometry relaxation of the $Ln(H_2O)_8^{3+}$ complex can be observed by calculating order parameters ($\theta_A$ and $\theta_B$), as proposed by Yazyev and Helm.[29] $\theta_A$ and $\theta_B$ are defined by the vectors connecting oxygen atoms of the inner sphere water molecules, as shown in Fig. 4 of Ref. 29. Calculated sets of order parameters for the $Ho(H_2O)_8^{3+}$ and $Lu(H_2O)_8^{3+}$, before and after a water exchange, were compared to those corresponding to the ideal SAP [$(\theta_A=22.5°,\ \theta_B=67.5°)$ and $(\theta_A=30.9°,\ \theta_B=55.3°)$] and DD [$(\theta_A=45°,\ \theta_B=45°)$ and $(\theta_A=25.5°,\ \theta_B=61.7°)$] geometries. The evolution of order parameters sets for the $Ho^{3+}$ first hydration shell shows that, before the water exchange, the first hydration shell might be in a nonideal DD geometry [Fig. 12(a)]. Getting closer to the water exchange, i.e., the incoming of the ninth water molecule in the first hydration shell, the nonideal DD geometry relaxes to a not well-defined geometry, which could be attributed to the BTP geometry since this geometry looks like the TTP one. After the water exchange, the first hydration shell relaxes to a non ideal DD geometry. Thus, after a water exchange, it seems that the first hydration shell of $Ho^{3+}$ has not enough time to full relax back to the SAP geometry. Concerning the first hydration of the $Lu^{3+}$ ion, the same profile of parameters, as calculated for $Ho^{3+}$, is found [Fig. 12(b)]. The difference
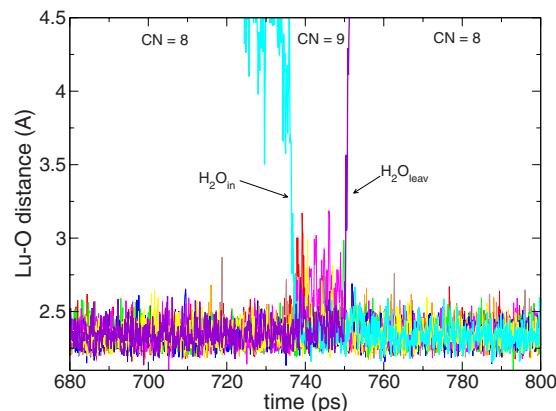


FIG. 9. (Color online) Gd–O distance of selected water molecules as a function of time.
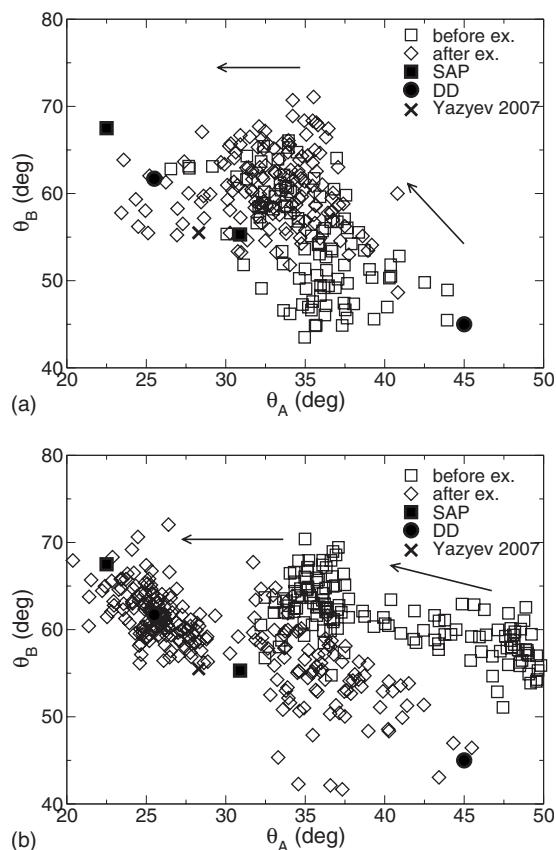


FIG. 11. (Color online) Lu–O distance of selected water molecules as a function of time.

FIG. 12. (a) Time evolution of the order parameters $\theta_A$ and $\theta_B$ of the Ho$^{3+}$ first hydration shell during a water exchange (1195 ps on Fig. 10). (b) Time evolution of the order parameters $\theta_A$ and $\theta_B$ of the Lu$^{3+}$ first hydration shell during a water exchange (750 ps on Fig. 11). The sets of parameters corresponding to the ideal SAP and trigonal, and the mean values of the parameters obtained for the Gd$^{3+}$ ion by Yazyev and Helm[29] (cross) are also shown.

observed concerns the relaxation of the geometry with 8 water molecules after the water exchange. Indeed, when the ninth water molecule leaves the first hydration shell, the geometry seems to be DD, which then can relax to the SAP geometry. Thus, for Lu$^{3+}$, since few water exchange occurs, the first hydration shell, in a DD geometry, has enough time to relax to the SAP geometry, in about 5 ps.

From this last analysis we can conclude that DD structure is a kind of intermediate structure that quickly relaxes to SAP when CN=8 is stable. This DD structure is also needed to allow the CN=8 complex make the room for an incoming ninth water molecule. This is done by a further changing of structure from DD to BTP-like when the incoming water is close to the lanthanoid.

## V. CONCLUSIONS

In this paper we have presented a pair interaction potential including explicit polarizability—by means of Thole's induced dipole model—suitable to address key questions about hydration structure and dynamics of the lanthanoid(III) series. In particular, the microscopic description obtained from MD simulations seems to be able to clarify some key points that are long debated in the literature. Namely, the changing of the CN across the series and the self-exchange

mechanism that is closely related to the knowledge of CN. We agree with recent experiments claiming the falling of the so-called gadolinium break model, with a turnover at the Tb$^{3+}$–Dy$^{3+}$ level, i.e., surprisingly in the middle between what proposed by Helm and Merbach[13]—they said that the Sm$^{3+}$ is the turning point—and what recently suggested by Persson et al.[14]—they said that the decreasing starts at Ho$^{3+}$ level. Note that our trend can be shifted toward Persson insights if the Ln(III) ionic radius employed to build the potential is bigger—corresponding to the use of CN=9 ionic radii instead of CN=8 ones. In fact, from our results one can clearly find that the ionic radius changing is the key physical parameters governing both structural—in terms of both Ln–O distances and CN—and dynamical properties. On the other hand, atomic polarizability seems to have a minor effect. These latter are in fact connected with the changeover of the relative stabilities of the two stoichiometries. Light lanthanoids have a ninefold structure with a TTP geometry as already observed for La$^{3+}$,[34] while moving across the series the eightfold structure becomes more probable and thermally populated. At the middle of the series we have a coexistence of two structures and at the end the eightfold one presents mainly a SAP geometry, as found for some high temperature La$^{3+}$ structure by us[49] and suggested previously.[13]

Analyzing water self-exchange dynamics across the series we are able to distinguish different self-exchange reactions and corresponding mechanisms depending on the position along the series.

(1) 9-10-9 reaction as for La$^{3+}$[34] for light lanthanoids with a concerted mechanism;
(2) 9-8-9 reaction for Nd$^{3+}$ with a concerted-associative mechanism. This becomes more probable moving across the series since the CN=8 structure becomes more stable.
(3) A thermodynamic equilibrium for the middle of the series, like for Gd$^{3+}$, such that it is not possible to identify a 9-8-9 or 8-9-8 reaction.
(4) A 8-9-8 reaction for the end of the series with a concerted-dissociative mechanism.

Note that this picture agrees with the proposed model of Helm and Merbach[13] for which across the series the mechanism changes from a concerted associative to a concerted-dissociative one. Of course, this holds for the 9-8-9 and 8-9-8 reactions, thus not at beginning of the series, where 9-10-9 self-exchange reactions are also noticed and in the middle where it is not possible to identify a clear self-exchange reaction.

Concluding, lanthanoids in water form two more stable structures, TTP for CN=9 and SAP for CN=8, and to go from one to the other they need to be distorted passing through some intermediate structures such as DD- and BTP-like. This relatively fast interexchanging between stoichiometries and structures with the same stoichiometry can be at the origin of the difficulty in interpreting experiments in absence of a full microscopic picture of lanthanoids series hydration provided in this work. A possible and suitable use of the proposed interaction potential and simulation data would

be the use for a direct coupling with EXAFS and XANES experiments in order to better explain those data in terms of microscopic properties.

## ACKNOWLEDGMENTS

[1] G. Chillemi, P. D'Angelo, N. Pavel, N. Sanna, and V. Barone, J. Am. Chem. Soc. **124**, 1968 (2002).

[2] C. Bresson, R. Spezia, S. Esnouf, P. Solari, S. Coantic, and C. Den Auwer, New J. Chem. **31**, 1789 (2007).

[3] A. Ruas, P. Guilbaud, C. Den Auwer, C. Moulin, J.-P. Simonin, P. Turq, and P. Moisy, J. Phys. Chem. A **110**, 11770 (2006).

[4] Y. An, M. T. Berry, and F. C. J. M. van Veggel, J. Phys. Chem. A **104**, 11243 (2000).

[5] P. D'Angelo, V. Migliorati, G. Mancini, V. Barone, and G. Chillemi, J. Chem. Phys. **128**, 084502 (2008).

[6] R. Spezia, M. Duvail, P. Vitorge, T. Cartailler, J. Tortajada, P. D'Angelo, and M.-P. Gaigeot, J. Phys. Chem. A **110**, 13081 (2006).

[7] R. Spezia, C. Bresson, C. Den Auwer, and M.-P. Gaigeot, J. Phys. Chem. B **112**, 6490 (2008).

[8] D. Hagberg, G. Karlstrom, B. O. Roos, and L. Gagliardi, J. Am. Chem. Soc. **127**, 14250 (2005).

[9] M. Buhl, H. Kabrede, R. Diss, and G. Wipff, J. Am. Chem. Soc. **128**, 6357 (2006).

[10] G. Mancini, N. Sanna, V. Barone, V. Migliorati, P. D'Angelo, and G. Chillemi, J. Phys. Chem. B **112**, 4694 (2008).

[11] B. M. Rode and T. S. Hofer, Pure Appl. Chem. **78**, 525 (2006).

[12] T. S. Hofer, H. T. Tran, C. F. Schwenk, and B. M. Rode, J. Comput. Chem. **25**, 211 (2004).

[13] L. Helm and A. E. Merbach, Chem. Rev. (Washington, D.C.) **105**, 1923 (2005).

[14] I. Persson, P. D'Angelo, S. D. Panfilis, M. Sandstrom, and L. Eriksson, Chem.-Eur. J. **14**, 3056 (2008).

[15] R. Silva, G. Bidoglio, M. Rand, P. Robouch, H. Wanner, and I. Puigdomenech, *Chemical Thermodynamics of Americium* (OECD, Paris, France, 2004).

[16] P. Vitorge and H. Capdevila, Radiochim. Acta **91**, 623 (2003).

[17] P. Vitorge, V. Phrommavanh, B. Siboulet, D. You, T. Vercouter, M. Descostes, C. J. Marsden, C. Beaucaire, and J.-P. Gaudet, C. R. Chimie **10**, 978 (2007).

[18] F. H. Spedding, M. J. Pikal, and B. O. Ayers, J. Phys. Chem. **70**, 2440 (1966).

[19] F. H. Spedding and K. C. Jones, J. Phys. Chem. **70**, 2450 (1966).

[20] F. H. Spedding and M. J. Pikal, J. Phys. Chem. **70**, 2430 (1966).

[21] L. Helm and A. E. Merbach, Eur. J. Solid State Inorg. Chem. **28**, 245 (1991).

[22] C. Cossy, L. Helm, D. H. Powell, and A. E. Merbach, New J. Chem. **19**, 27 (1995).

[23] T. S. Hofer, H. Scharnagl, B. R. Randolf, and B. M. Rode, Chem. Phys. **327**, 31 (2006).

[24] C. Clavaguera, F. Calvo, and J.-P. Dognon, J. Chem. Phys. **124**, 074505 (2006).

[25] T. Kowall, F. Foglia, L. Helm, and A. E. Merbach, J. Am. Chem. Soc. **117**, 3790 (1995).

[26] T. Kowall, F. Foglia, L. Helm, and A. E. Merbach, J. Phys. Chem. **99**, 13078 (1995).

[27] F. M. Floris and A. Tani, J. Chem. Phys. **115**, 4750 (2001).

[28] T. Ikeda, M. Hirata, and T. Kimura, J. Chem. Phys. **122**, 244507 (2005).

[29] O. V. Yazyev and L. Helm, J. Chem. Phys. **127**, 084506 (2007).

[30] C. Cossy, L. Helm, and A. E. Merbach, Inorg. Chem. **27**, 1973 (1988).

[31] B. P. Hay, Inorg. Chem. **30**, 2876 (1991).

[32] S. Chaussedent, A. Monteil, M. Ferrari, and L. D. Longo, Philos. Mag. B **77**, 681 (1998).

[33] J. Näslund, P. Lindqvist-Reis, I. Persson, and M. Sandström, Inorg. Chem. **39**, 4006 (2000).

[34] M. Duvail, M. Souaille, R. Spezia, T. Cartailler, and P. Vitorge, J. Chem. Phys. **127**, 034503 (2007).

[35] S. Diaz-Moreno, A. Munoz-Paez, and J. Chaboy, J. Phys. Chem. A **104**, 1278 (2000).

[36] M. Duvail, P. D'Angelo, M. Gaigeot, P. Vitorge, and R. Spezia, Radiochim. Acta, in press (2009).

[37] M. Duvail, R. Spezia, and P. Vitorge, ChemPhysChem **9**, 693 (2008).

[38] B. T. Thole, Chem. Phys. **59**, 341 (1981).

[39] W. L. Jorgensen, J. Chandrasekhar, J. D. Madura, R. W. Impey, and M. L. Klein, J. Chem. Phys. **79**, 926 (1983).

[40] A. J. Stone, *The Theory of Intermolecular Forces, International Series of Monographs on Chemistry* (Clarendon, Oxford, 1997), Vol. 32.

[41] H. L. Williams, K. Szalewicz, B. Jeziorski, R. Moszynski, and S. Rybak, J. Chem. Phys. **98**, 1279 (1993).

[42] *Handbook of Physics and Chemistry* (CRC, Boca Raton, Fl, 1996).

[43] R. D. Shannon, Acta Crystallogr., Sect. A: Cryst. Phys., Diffr., Theor. Gen. Crystallogr. **32**, 751 (1976).

[44] F. Hutchinson, M. Wilson, and P. A. Madden, Mol. Phys. **99**, 811 (2001).

[45] M. Salanne, C. Simon, P. Turq, and P. A. Madden, J. Phys. Chem. B **112**, 1177 (2008).

[46] M. Souaille, H. Loirat, D. Borgis, and M.-P. Gaigeot, Comput. Phys. Commun. **180**, 276 (2009).

[47] M. Sprik, J. Phys. Chem. **95**, 2283 (1991).

[48] U. Essmann, L. Perera, M. L. Berkowitz, T. Darden, H. Lee, and L. G. Pedersen, J. Chem. Phys. **103**, 8577 (1995).

[49] M. Duvail, R. Spezia, T. Cartailler, and P. Vitorge, Chem. Phys. Lett. **448**, 41 (2007).

[50] M. J. Frisch, G. W. Trucks, H. B. Schlegel *et al.*, GAUSSIAN 98, Revision A.9 Gaussian, Inc., Pittsburgh, PA, 1998.

[51] P. C. Hariharan and J. A. Pople, Theor. Chim. Acta **28**, 213 (1973).

[52] S.-I. Ishiguro, Y. Umebayashi, K. Kato, R. Takahashib, and K. Ozutsumi, J. Chem. Soc., Faraday Trans. **94**, 3607 (1998).

[53] T. Yaita, H. Narita, S. Suzuki, S. Tachimori, H. Motohashi, and H. Shiwaku, J. Radioanal. Nucl. Chem. **239**, 371 (1999).

[54] T. Yamaguchi, M. Nomura, H. Wakita, and H. Ohtaki, J. Chem. Phys. **89**, 5153 (1988).

[55] A. Habenschuss and F. H. Spedding, J. Chem. Phys. **70**, 2797 (1979).

[56] R. D. Rogers and L. K. Kurihara, Inorg. Chim. Acta **130**, 131 (1987).

[57] W. Meier, P. Bopp, M. M. Probst, E. Spohr, and J. L. Lin, J. Phys. Chem. **94**, 4672 (1990).

[58] C. Cossy, L. Helm, and A. E. Merbach, Inorg. Chem. **28**, 2699 (1989).

[59] J. K. Burdett, R. Hoffmann, and R. C. Fay, Inorg. Chem. **17**, 2553 (1978).

[60] M. Kotzian and N. Roesch, J. Phys. Chem. **96**, 7288 (1992).

[61] A. Habenschuss and F. H. Spedding, J. Chem. Phys. **70**, 3758 (1979).

[62] J. A. Solera, J. Garcia, and M. G. Proietti, Phys. Rev. B **51**, 2678 (1995).

[63] P. Allen, J. J. Bucher, D. K. Shuh, N. M. Edelstein, and I. Craig, Inorg. Chem. **39**, 595 (2000).